JOURNAL OF THERMOPLASTIC COMPOSITE MATERIALS

Original research article

Tailored PLA/Chitosan/MCC composite filaments for fused filament fabrication

Journal of Thermoplastic Composite Materials
2026, Vol. 0(0) 1–25

DOI: 10.1177/08927057261458264
journals.sagepub.com/home/jtc
Sage

The Jaya Suteja[1], Natalia Soeseno[2], Akbarningrum Fatmawati[2], Emma Savitri[2] and Yuli Panca Asmara[3]

Abstract

The growing demand for patient-specific orthopedic implants has accelerated the development of polymer-based materials suitable for fused filament fabrication (FFF). This study aims to develop composite filaments based on polylactic acid (PLA), chitosan, and microcrystalline cellulose (MCC) for FFF applications in orthopedic implants. The composites were synthesized via melt blending and extrusion, with variations in chitosan content (1–2 wt%), MCC content (3–5 wt%), and extrusion temperature (155–165°C). Characterization included rheological testing (MFR), structural analysis (FTIR, XRD), morphological observation (SEM-EDX), thermal properties (TGA, DSC), and water absorption. The results indicate that the addition of chitosan and MCC does not alter the chemical structure of PLA but enhances interfacial interactions through hydrogen bonding. Chitosan acts as a compatibilizer, improving MCC dispersion and matrix–filler adhesion. Melt flow properties are governed by the balance between PLA content, filler composition, and extrusion temperature. All composites exhibit sufficient thermal stability for FFF; however, increasing filler content and extrusion temperature leads to higher water absorption. The optimum composition was achieved at 93 wt% PLA, 2 wt% chitosan, and 5 wt% MCC at an extrusion temperature of 155°C, yielding the most balanced performance. These findings provide mechanistic insight into the potential product innovation of composite filaments for future FFF-based orthopedic implants.

[1]Department of Mechanical Engineering, University of Surabaya, Raya Kalirungkut, Surabaya, Indonesia
[2]Department of Chemical Engineering, University of Surabaya, Surabaya, Indonesia
[3]Department of Mechanical Engineering, Faculty of Engineering & Quantity Surveying, INTI International University, Nilai, Negeri Sembilan, Malaysia

Corresponding author:
The Jaya Suteja, Department of Mechanical Engineering, University of Surabaya, Raya Kalirungkut, Surabaya 60292, Indonesia.
Email: jayasuteja@staff.ubaya.ac.id

Keywords
PLA, Chitosan, MCC, composite, fused filament fabrication

Introduction

The increasing human life expectancy has led to an increase in bone fracture cases due to decreased bone density and quality associated with aging.[1] Conventional bone repair surgery typically relies on internal fixation methods that require specialized implants. Internal fixation commonly employs implants such as plates, pins, or screws placed within the body to stabilize fractured bones. Ideally, the shape and size of these implants should be customized to accommodate various fracture patterns and the unique geometry of each patient's bone.[2] Commonly used implant materials include metals such as stainless steel and titanium, which offer corrosion resistance, biocompatibility, and excellent mechanical performance. While these metallic implants provide robust and stable bone fixation, they also present several drawbacks, including limited formability, high cost, potential damage to surrounding tissues, reduced bone density, and complications during removal.[3,4]

In addition to metals, polymer-based materials have emerged as promising alternatives due to their ease of fabrication and lower cost. Polymer implants must retain the advantageous properties of metallic implants while also offering additional benefits, such as antimicrobial and biodegradability characteristics.[5] An antimicrobial characteristic is required, as implant placement carries an inherent risk of infection at the implantation site.[6] Once bone healing is complete, implants are typically removed, but removal procedures pose risks of damage to bone and surrounding tissues.[7] Conversely, leaving implants in place may lead to adverse effects and impede bone development, particularly in pediatric patients.[8] Therefore, polymer implants should ideally be biodegradable and capable of being resorbed by the body to minimize discomfort and prevent long-term complications for patients.[9,10]

Drawing upon the aforementioned considerations, this study addresses the critical need for alternatives to metallic internal fixation. The solution proposed in this study is to use a Polylactic Acid (PLA)/Chitosan/Cellulose composite material to fabricate implants. Previous studies have employed composite materials for implant fabrication with PLA as the matrix polymer.[11,12] The selected matrix material is PLA due to its biocompatibility, biodegradability, and bioabsorbability.[13–16] PLA undergoes hydrolytic degradation to lactic acid or carbon dioxide and water, which are subsequently absorbed by the body and eliminated via urine or respiration.[17] In addition, PLA is selected because it exhibits superior mechanical properties compared to other biodegradable polymers.[18] Even though its mechanical strength remains lower than that of human bone,[19] PLA can retain its strength for up to 8 weeks.[20]

The hydrolysis of PLA may increase local acidity and elevate the risk of infection around the implant site.[20] Therefore, implant materials must also possess antimicrobial properties to mitigate the risk of infection.[21,22] To address this, the present study incorporates chitosan into PLA to impart antimicrobial activity.[23–25] Chitosan has been

incorporated into PLA to reduce infection risks, given that chitosan is an antimicrobial, biocompatible, biodegradable, non-toxic, and non-allergenic polymer.[26–28] Although the addition of chitosan can lower the risk of infection, it also reduces certain mechanical properties of PLA/Chitosan composites.[21,26,29,30]

Various approaches have been explored to enhance PLA's mechanical performance.[31–33] One of which is cellulose reinforcement to improve the mechanical strength of polymer composites.[33–36] Several studies have incorporated Microcrystalline Cellulose (MCC) into PLA to enhance the mechanical performance of PLA-based composites.[37–39] MCC reinforcement has been shown to improve the mechanical and thermal properties as well as the crystallinity of PLA.[40] Other studies have reported that the inclusion of Cellulose Nanocrystals (CNC) can also increase the tensile strength of PLA.[41] The cellulose–chitosan blends have been developed to combine the mechanical strength, water stability, and hydrophilicity of cellulose with the antimicrobial properties of chitosan.[42] Owing to its biocompatibility and mechanical integrity, the PLA/Chitosan/Cellulose composite represents a promising candidate for internal fixation applications in orthopedic surgery.

The addition of cellulose to PLA/Chitosan composites has also been explored using the solvent casting method for packaging coatings.[43] However, this method is unsuitable for producing implants intended for internal fixation, which require high mechanical strength, precision, and specific structural characteristics.[44] Three-dimensional (3D) printing has increasingly been used to fabricate polymer implants for both internal and external fixation.[3,45–48] This technology enables the rapid and precise production of implants tailored to the fracture and the patient's bone geometries. Mechanical improvements in PLA/Chitosan composites can be achieved by optimizing 3D printing parameters.[29] Previous studies have demonstrated that antimicrobial PLA-based composites can be processed via 3D printing,[49] and PLA prints can be effectively sterilized by methods such as autoclaving or gamma irradiation.[24]

One of the 3D printing technologies, Fused Filament Fabrication (FFF), has been widely used to fabricate polymer products. Therefore, FFF will be used to produce internal fixation implants made of a PLA/Chitosan/Cellulose composite filament. In this study, the filament was fabricated via melt blending followed by extrusion. Consequently, the PLA/Chitosan/Cellulose composite must demonstrate sufficient processability for melt extrusion to facilitate filament fabrication.

While PLA-based composites incorporating chitosan and cellulose have been investigated, existing studies predominantly address binary systems, solvent-cast materials, or bulk property characterization, with limited focus on filament processability for FFF. Furthermore, the combined effects of composition and processing conditions on the printability and performance of PLA/chitosan/MCC systems remain poorly understood.

To provide a comprehensive solution to the challenge above, the following research questions are formulated:

> How to synthesize the PLA/Chitosan/Cellulose composite that satisfies the requirements for filament fabrication?

To what extent do the tailored PLA/Chitosan/Cellulose composites exhibit the requisite properties for filament of FFF?

This study addresses these gaps by developing a PLA/Chitosan/Cellulose composite tailored for use as an FFF filament and establishing a composition–processing–property relations. Specifically, this research aims to:

Develop a synthesis method for PLA/Chitosan/Cellulose composites that meets the requirements for filament fabrication.
Characterize the properties of the tailored PLA/Chitosan/Cellulose composites to be used as filament for FFF.

This study presents an approach for tailoring PLA/Chitosan/Cellulose composite filaments via melt blending and extrusion to meet the processing and stability requirements of FFF. By correlating composite composition and extrusion temperature with melt-flow behavior, morphological stability, thermal resistance, and water uptake, this study identifies a balanced processing window for FFF filaments. The work provides mechanistic insight into the composition–processing–property relationships that govern filament performance. The resulting composite filaments offer potential material for future biomedical and orthopedic manufacturing applications.

Materials and Methods

Materials

Ingeo™ Biopolymer 4043D PLA, manufactured by NatureWorks, was used in this study. This type of PLA is well-suited for a broad range of applications.[50] The melt flow index of this PLA grade is reported to be 6 g/10 min according to ASTM D1238 (210°C, 2.16 kg), with a specific gravity of 1.24 g/cm^3 according to ASTM D792. The selection of Ingeo™ 4043D represents a strategic compromise between processability during filament extrusion and dimensional accuracy. Furthermore, this study used low molecular weight chitosan (Sigma Aldrich, Product Number: 448869, CAS Number: 9012-76-4) in the form of powder. Low-molecular-weight chitosan is selected because it provides superior biodegradability and bioactivity compared to high-molecular-weight chitosan.[51] Last, the cellulose used in this research, in form of MCC powder, was supplied by Merck (Part Number: 1.02331.0500, particle size between 10 μm and 160 μm). The rigid, crystalline structure of MCC enables efficient load-bearing and stress transfer from the polymer matrix.[52]

Fabrication of PLA/Chitosan/MCC Composite Filaments

To synthesize the PLA/Chitosan/MCC composite that meets the requirements for filament fabrication, the processes performed in this study are presented in Figure 1. First, all materials are continuously stirred at room temperature to create a PLA/Chitosan/MCC

mixture. To prevent hydrolytic degradation during processing and minimize moisture-induced defects, the material mixture was subjected to a standardized dehydration process in a vacuum oven at 55°C for 2 hours before melt-blending. Then, the mixture was processed in a single-screw extruder (ReDeTec Protocycler) at a certain extrusion temperature. The extruder rotation speed was set to 30 rpm during filament production. Based on the previous study, chitosan content was strategically limited to 1–2 wt% to maintain optimal extrudability and prevent nozzle clogging,[26] while cellulose was incorporated at 3–5 wt% to reinforce the crystalline structure and enhance thermal stability.[33,53] An extrusion temperature of 155–165°C was selected, based on the PLA melting point identified via DSC analysis and preliminary experimental optimization, to ensure consistent melt rheology during extrusion. Four formulations were investigated by varying the concentrations of PLA, chitosan, and MCC, as well as the extrusion temperature, as detailed in Table 1. Figure 2 shows the physical image of four compositions of the composite.

Characterizations

The suitability of the four PLA/Chitosan/MCC composite formulations for FFF filament was evaluated through a series of comprehensive characterizations described below.

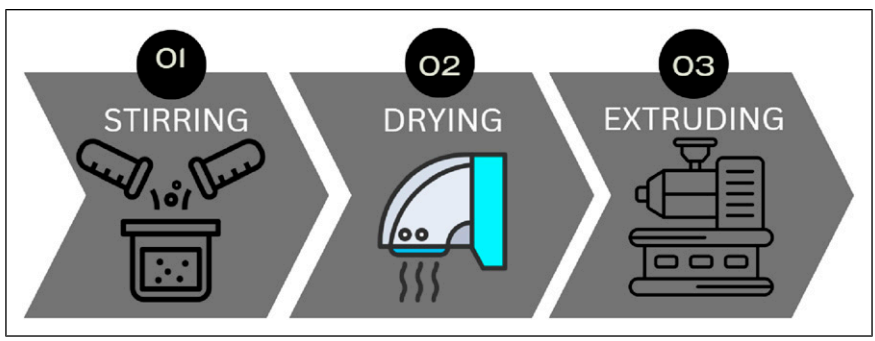

Figure 1. Schematic overview.

Table 1. Composition of composites.

Composite	Chitosan (wt. %)	MCC (wt. %)	PLA (wt. %)	Extrusion temperature (°C)
A	1	3	96	155
B	1	5	94	155
D	2	5	93	155
H	2	5	93	165

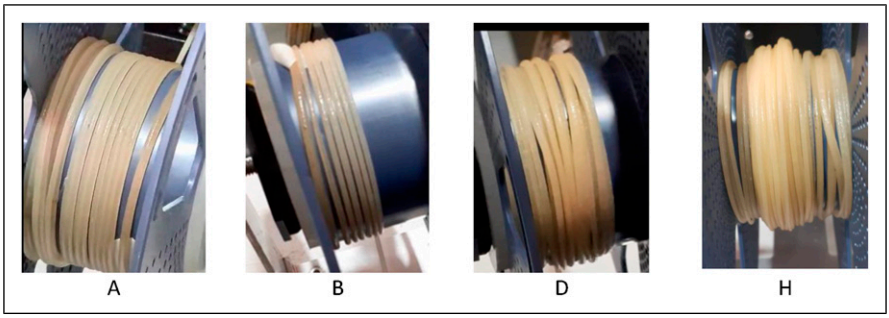

Figure 2. Physical image of the composites.

Rheological Analysis. The Melt Flow Rate of the composite was measured to assess the melt viscosity and flow behavior during extrusion using the Mflow Extrusion Plastometer (ZwickRoell).

Structural and Morphological Analysis. Fourier Transform Infrared Spectroscopy (IRTracer–100, Shimadzu) was used to investigate intermolecular interactions and hydrogen bonding. The crystalline phase and constituent identification were performed using X-ray Diffraction (Aeris Benchtop, Malvern Panalytical), and the surface topography was examined using Scanning Electron Microscopy (Axia ChemiSEM, Thermo Scientific).

Thermal Analysis. Differential Scanning Calorimetry (Mettler Toledo) was conducted to evaluate the glass transition temperature (Tg) and melting temperature (Tm). Thermogravimetric Analysis (STA 6000, PerkinElmer) was used to determine the thermal decomposition kinetics.

Water Absorption Analysis. Water absorption capacity was quantified in accordance with ISO 62 at ambient temperature.

Results and Discussion

The next stage involved analyzing the physicochemical data resulting from the characterization above. The results were validated against the properties required for FFF implementation.

Rheological Analysis

The results of Melt Flow Rate (MFR) testing are shown in Table 2 below. PLA serves as the continuous melt phase, forming an entangled polymer network that dominates melt viscosity. Composites with a higher PLA fraction (e.g., Composite A) tend to exhibit lower MFR because the polymer chains form more entanglements that resist flow under

Table 2. MFR of composites.

Composite	MFR (g/10 min)
A	9.54
B	14.38
D	10.55
H	13.52

shear. Conversely, lowering PLA content reduces the entanglement density, thereby facilitating molecular mobility and enhancing melt flowability. This effect is consistent with the understanding that lower chain-entanglement density reduces viscous resistance in polymer melts.

Although rigid fillers such as MCC are usually associated with increased melt viscosity due to geometric hindrance and restricted polymer chain mobility, in some multicomponent systems, their effect may be offset or modified by other mechanisms. For example, incorporating MCC at moderate loadings (e.g., Composite B) can sufficiently disrupt polymer network continuity that the effective continuous PLA phase fraction decreases noticeably, yielding a net increase in MFR despite the presence of the rigid filler. Examination of PLA composites with varying MCC levels has shown that MCC can influence rheological properties by altering polymer chain disentanglement and flow-regime transitions, as well as changes in crystallinity and matrix mobility. A study on PLA/MCC composites prepared via melt blending reports variations in rheological behavior with filler content that align with these trends and emphasizes how filler dispersion and interactions with plasticizers affect melt processability.[54]

The presence of chitosan introduces additional intermolecular interactions (e.g., hydrogen bonding) that can affect the mobility of PLA chains and the dispersion of MCC particles. An increase in chitosan from 1% to 2% (e.g., Composite D vs Composite B) at the same MCC content and temperature was associated with a lower MFR, suggesting that chitosan may enhance cohesive interactions in the melt, increasing melt viscosity or reducing chain mobility. Such effects have been discussed in broader studies of PLA blends and biopolymer composites containing chitosan, where chitosan alters melt characteristics through its influence on matrix structure and rheological response.[55]

Processing temperature directly affects melt viscosity and, in turn, the resulting MFR/MVR values. Higher extrusion temperatures reduce melt viscosity by increasing polymer chain mobility and diminishing entanglements and cohesive forces, as evidenced by the increased MFR of Composite H (extruded at 165°C) compared to Composite D (extruded at 155°C), despite similar compositions. This is consistent with the general principle that melt flow indices increase with processing temperature due to thermal softening and decreased resistance to flow.[56]

The rheological characterization of the composites above reveals a significant variance in flow behavior. A threshold value of 10 g/10 min (based on ISO 1133) is required to enable a good printing process and enhance inter-layer diffusion of the composite using a 190 - 220°C nozzle temperature.[57] Composite B and composite H exhibited the

highest fluidity, placing them well above the threshold and suggesting superior molecular mobility that enhances layer adhesion. Composite D closely aligns with the recommended benchmark, indicating a balanced profile between flowability and structural stability. Conversely, composite A falls slightly below the threshold, potentially necessitating higher processing temperatures to achieve the rheological performance required for high-strength fusion.

Structural and Morphological Analysis

Fourier Transform Infrared (FTIR) Spectroscopy Analysis. FTIR spectroscopy was employed to elucidate the chemical structure and interfacial interactions of PLA and PLA/Chitosan/MCC composite filaments with different filler compositions. FTIR spectra of PLA and PLA/Chitosan/MCC composite are shown in Figure 3.

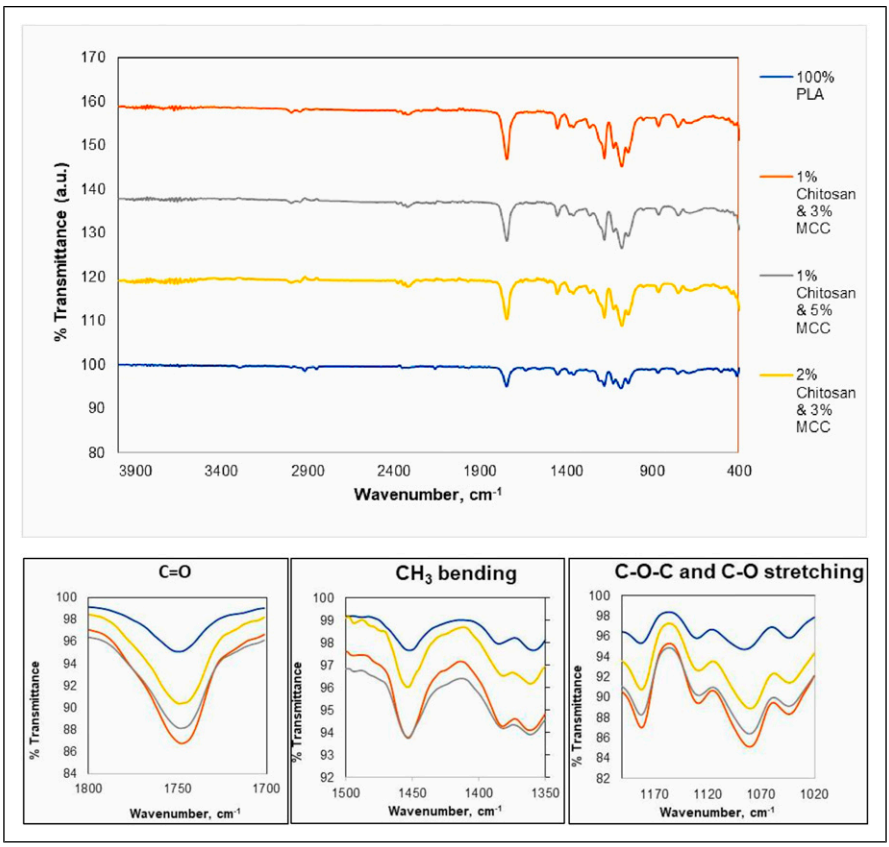

Figure 3. FTIR spectra of PLA and PLA/Chitosan/MCC composite.

All composite spectra are dominated by the characteristic absorption bands of PLA, which is consistent with the high PLA content (>94 wt%) in all formulations. The intense ester carbonyl band at 1750 cm^{-1} is preserved in all composites, indicating that the incorporation of chitosan and MCC does not alter the chemical backbone of PLA. Additional PLA-related bands, including C–H stretching vibrations at 3000–2950 cm^{-1} and CH_3 bending vibrations at 1450 and 1360–1380 cm^{-1}, remain unchanged across all composites. These observations are in good agreement with previous studies on PLA/Cellulose and PLA/Chitosan bio-composites, which consistently report the absence of new absorption peaks and the preservation of the PLA ester functionality, suggesting that the interactions between PLA and polysaccharide fillers are predominantly physical rather than chemical in nature.[58–60]

The contribution of polysaccharide components is mainly reflected in the broad absorption region at 3400–3200 cm^{-1} and in the fingerprint region (1200–900 cm^{-1}). The broadening of the O–H or N–H stretching band becomes more pronounced in the composite filaments, particularly in the composite with higher MCC content and the composite with higher chitosan content, indicating enhanced intermolecular hydrogen bonding between PLA carbonyl groups and hydroxyl or amino groups of the fillers. In the fingerprint region, PLA exhibits strong C–O–C and C–O stretching bands at 1184 and 1080 cm^{-1}, while the composites show broader and more complex features due to overlapping contributions from polysaccharide backbones. Composite with higher MCC content displays the most significant modification, with enhanced shoulders at 1050–1020 cm^{-1} characteristic of cellulose C–O stretching and contributions near 900 cm^{-1} associated with β-glycosidic linkages, consistent with reports on PLA/MCC systems where increasing cellulose content intensifies polysaccharide-related fingerprint features.[59,60] In contrast, composite with higher chitosan exhibits subtle features in the 1650–1550 cm^{-1} region attributable to residual amide I and amide II vibrations of chitosan, in line with previous observations for PLA/Chitosan composites.[61,62]

The FTIR analysis demonstrates that incorporating MCC and chitosan into the PLA matrix does not induce new chemical functionalities but instead promotes intermolecular hydrogen bonding and other physical interactions at the polymer–filler interface. These interactions are strongly dependent on filler composition and are manifested primarily through peak broadening and modifications in the fingerprint region sensitive to polysaccharides. Such composition-dependent interfacial interactions are expected to influence the structural organization and subsequent thermal and mechanical behavior of the composite filaments.

X-ray Diffraction (XRD) Analysis. The result of baseline-corrected XRD curves is shown in Figure 4. The four composites exhibit amorphous material. Peaks are especially evident for composites B and H. However, the peaks are very broad, which is characteristic of amorphous materials. The diffraction peaks observed in the XRD patterns represent well-ordered crystallites that act as effective reinforcing agents and are directly correlated with enhanced mechanical stiffness and tensile modulus.[63] However, increased crystallinity often correlates with diminished interlayer adhesion due to the rapid solidification of polymer chains at the printing interface.[64]

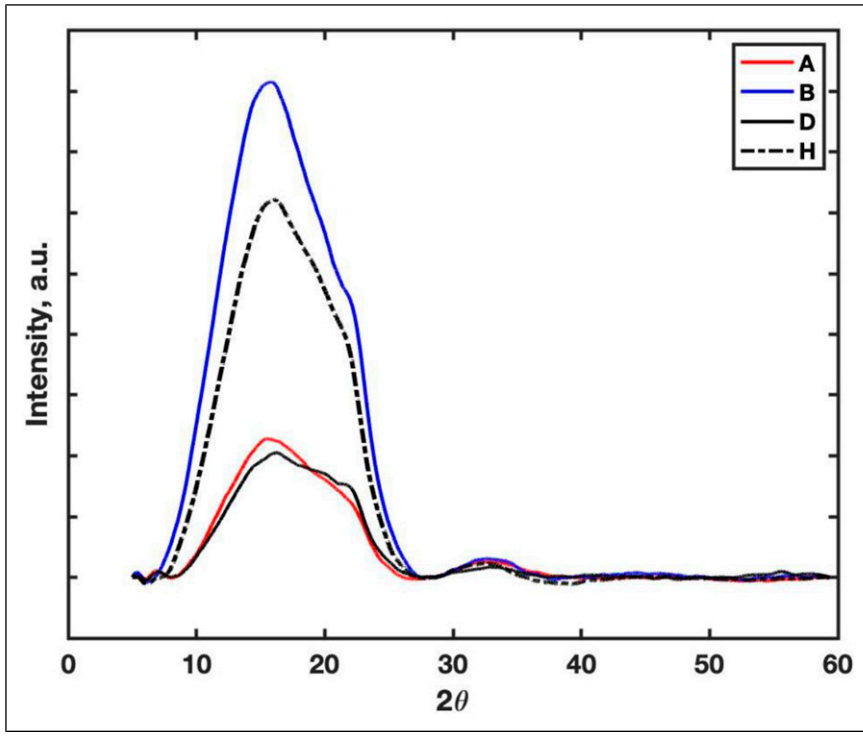

Figure 4. X-ray diffraction profiles of PLA/Chitosan/MCC composite.

According to Mazzanti et al., crystalline PLA showed an intense peak at $2\theta = 17^o$ while its composites with hemp fiber were amorphous.[65] Rapid cooling of the molten composite may result in the formation of amorphous composites. Nevertheless, the amorphous composites still enhance PLA's tensile strength. The diffractogram in Figure 4 also showed a very broad amorphous peak at 17^o. The peak combined with those of MCC and chitosan at 22^o and 20^o, respectively.[66] The presence of well-defined diffraction peaks across all composite formulations indicates their potential as functional FFF filaments, despite variations in crystallinity.

Scanning Electron Microscopy (SEM) Analysis. SEM was used to investigate the fracture-surface morphology of PLA and PLA/Chitosan/MCC composite filaments with four different compositions. These SEM micrographs of PLA/Chitosan/MCC composite filaments are shown in Figure 5 below.

For composition A, the fracture surface is relatively smooth, compact, and continuous, indicating that the PLA matrix remains the dominant structural phase. The low MCC content limits filler–filler interactions, allowing MCC to be reasonably well dispersed within the matrix. Only a small number of microvoids are observed, and no extensive filler pull-out is evident. Similar morphologies have been reported by Fortunati et al. and

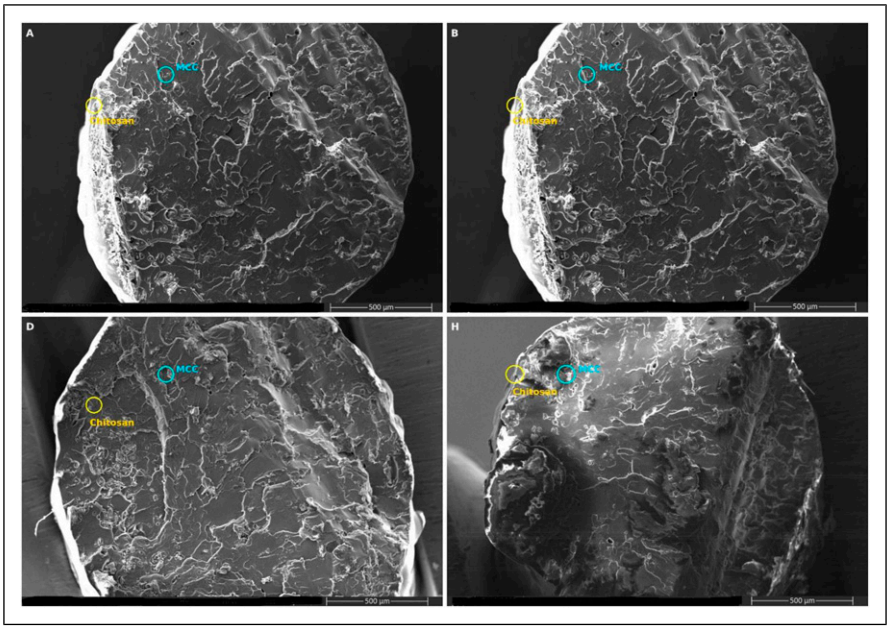

Figure 5. SEM micrographs of PLA/Chitosan/MCC composite filaments prepared at different compositions and extrusion temperatures.

Oksman et al. for PLA/MCC composites with low cellulose content, where good dispersion and matrix continuity are maintained.[67,68] The presence of chitosan, even at low concentrations, likely improves interfacial cohesion through hydrogen bonding with MCC, as also reported in PLA/Chitosan systems by Rhim, Park, and Ha.[69]

When the MCC content is increased to 5 wt% while maintaining chitosan at 1 wt% (e.g., composition B), the fracture surface becomes markedly rougher and more heterogeneous, with visible microvoids, irregular cavities, and features associated with filler pull-out. This morphology indicates MCC agglomeration and interfacial debonding, which are commonly observed when cellulose loading exceeds the dispersion limit in PLA matrices. Comparable SEM features, such as voids and clustered cellulose domains, have been widely reported in PLA/MCC composites by Fortunati et al. and Oksman et al., who attributed these defects to strong hydrogen bonding between cellulose particles and to insufficient interfacial compatibility with PLA.[67,68] In the current composite, the limited chitosan content is insufficient to effectively cover the increased MCC surface area, resulting in weak interfacial regions.

A clear morphological improvement is observed when the chitosan content is increased to 2 wt% while keeping the MCC loading constant (e.g., composition D). Compared to composition B, the fracture surface exhibits finer microstructural features, reduced void size, and a more cohesive fracture pattern. This indicates enhanced interfacial adhesion and improved filler wetting. Similar effects of chitosan acting as a

natural compatibilizer have been reported in PLA/Chitosan and PLA/Chitosan/MCC systems, where increased chitosan content promotes hydrogen bonding and reduces interfacial gaps.[58,69] The present SEM results confirm that chitosan partially mitigates MCC-induced agglomeration by forming a chitosan-mediated interphase between MCC and PLA.

Despite having identical compositions, composites D and H exhibit noticeable microstructural differences attributable to the variation in extrusion temperature. Composite H, processed at the higher temperature (165°C), displays localized regions of pronounced surface roughness and occasional filler-enriched domains, suggesting temperature-induced changes in melt flow behavior and phase redistribution during processing. In contrast, composite D (155°C) exhibits comparatively more uniform dispersion, indicating that moderate processing temperatures may favor improved phase stabilization in this composite. This behavior is consistent with recent reports on PLA/Cellulose composites, where processing temperature modulates melt viscosity, interfacial wetting, and shear-induced dispersion dynamics.[70,71] While elevated temperatures may enhance polymer–filler contact through improved chain mobility, excessive thermal energy can simultaneously promote filler migration or re-agglomeration, particularly in high-MCC formulations. Such temperature-dependent morphological variability in cellulose-reinforced PLA composites has been widely reported. Oksman et al. emphasized the high sensitivity of PLA/Cellulose composites to processing conditions, particularly shear history, residence time, and moisture content, all of which influence filler dispersion and interfacial adhesion.[68] Elevated extrusion temperatures can reduce melt viscosity and enhance wetting of polysaccharide fillers; however, excessive thermal mobility may also promote filler migration or partial re-agglomeration, especially in composites with high MCC loading.

The present observations suggest that while chitosan enhances interfacial compatibility through hydrogen-bond-mediated interactions with both PLA and MCC, MCC remains the dominant factor governing morphological stability due to its intrinsic tendency to form hydrogen-bonded networks. Compared with previously reported PLA/MCC composites lacking compatibilizers, the PLA/Chitosan/MCC composites investigated here demonstrate reduced interfacial voids and improved matrix–filler cohesion, particularly at optimized processing temperatures. Nevertheless, complete suppression of MCC aggregation likely requires additional strategies, such as surface-modified cellulose or reactive compatibilization approaches, as suggested by Oksman et al. and Farah, Anderson and Langer.[58,68]

Elemental composition analysis using SEM–EDX confirms that carbon (C), oxygen (O), and nitrogen (N) are the dominant elements in all PLA/Chitosan/MCC composite filaments, consistent with the chemical structures of PLA and polysaccharide constituents. Quantitative results reveal that composite A contains 49.3 at.% C, 44.1 at.% O, and 6.6 at.% N. Increasing the MCC fraction in composite B slightly elevates nitrogen to 8.2 at.%, whereas composite D shows 6.1 at.% N. Notably, composite H exhibits 7.7 at.% N, despite having an identical composition to D, indicating that extrusion temperature influences the detectable surface distribution of chitosan-rich domains. Because nitrogen originates exclusively from chitosan due to its primary amine groups, the N atomic

percentage serves as a reliable tracer for chitosan dispersion within the PLA/MCC matrix. The relatively higher nitrogen content observed in composite B and H suggests localized enrichment or improved surface exposure of chitosan under those processing conditions. The increase in detectable N at 165°C (composite H) may be attributed to enhanced polymer chain mobility during extrusion, which can promote the redistribution of the chitosan phase toward fracture surfaces, as examined by SEM. Similar temperature-dependent elemental redistribution in PLA/Cellulose composites has been reported in recent studies, where melt viscosity reduction at elevated processing temperatures influenced filler migration and phase exposure.[70,71] However, excessive thermal energy can also induce partial re-agglomeration of cellulose-rich domains, as observed in high-loading composites.[59] The carbon and oxygen ratios remain relatively stable across the composites (C ≈ 48–51 at.% and O ≈ 43–44 at.%), reflecting the dominant contribution of the PLA matrix. Minor variations in C/O balance are attributable to differences in MCC content, since cellulose has a higher oxygen-to-carbon ratio than PLA. The stability of these elemental ratios further supports the FTIR findings that no new covalent bonding occurred during compounding, as no additional heteroatoms were introduced beyond those intrinsic to the polymer components. Instead, the interaction mechanism remains dominated by hydrogen bonding between PLA carbonyl groups and hydroxyl/amino groups of MCC and chitosan, consistent with recent spectroscopic and morphological studies on PLA–polysaccharide composites.[72,73] Elemental mapping also confirms a relatively homogeneous spatial distribution of C and O throughout the matrix, whereas N mapping shows localized yet well-dispersed domains corresponding to chitosan-rich regions. Compared with previously reported PLA/MCC composites without compatibility, the present PLA/Chitosan/MCC composites display reduced elemental clustering and fewer nitrogen-depleted interfacial voids, indicating improved matrix–filler cohesion. Nevertheless, the persistence of localized compositional heterogeneity, particularly at higher MCC loadings, suggests that MCC remains the dominant factor governing morphological stability, owing to its intrinsic tendency to form hydrogen-bonded networks.[74] The EDX results corroborate the SEM morphological observations and FTIR interfacial analysis, demonstrating that chitosan functions primarily as a compatibilizing interphase that enhances elemental homogeneity and interfacial continuity. However, complete suppression of MCC aggregation would likely require further strategies such as surface-modified cellulose, reactive compatibilization, or optimized extrusion rheology, as proposed in recent polysaccharide-reinforced PLA composites.[59,70]

Despite the localized filler agglomeration observed at higher MCC loadings, the SEM and EDX analyses confirm that all developed composites maintain a continuous PLA matrix and sufficient interfacial cohesion. These findings, combined with the successful elemental distribution of nitrogen as a tracer for chitosan, demonstrate that all formulations are viable candidates for FFF filament production, with composition D representing the most morphologically optimized system.

Thermal Analysis

Thermogravimetric Analysis (TGA). TGA is used to assess thermal stability as a function of temperature. The study of the thermal stability of polymer or composite materials is

important for developing processing strategies, identifying potential applications, and thermal recycling of polymers. Figure 6 shows the thermogram of four composites studied in this research. All the composites behave relatively the same, although composite H shows very slightly more thermal stability compared to the other three composites. The first and only large drop in weight (90%) occurred at 340°C. This one-stage decomposition was also confirmed for pure PLA at 260-300°C. The PLA-cotton byproduct, containing a biocomposite, also exhibited one-step decomposition.[60] All the composites in this work were almost completely devolatilized at 380°C. Similar behavior was observed in pure PLA.[60,75] This thermal behavior information for the composites is important, as the filament composites will be processed in a 3D printer to produce final, usable products. As filament composites can withstand temperatures above 300°C, they are potentially suitable for use in 3D printing.

Differential Scanning Calorimetry (DSC) Analysis. DSC is used to evaluate the effect of chitosan and cellulose on glass transition temperature (Tg), melting temperature (Tm), and degree of crystallinity (Xc). The DSC thermograms of the studied biocomposites are shown in Figure 7. The thermograms show how the composite's heat flow changes with temperature. Composites A, B, and D show a similar trend, while composite H behaves differently. However, as shown in Table 3, the values of the glass transition and melting

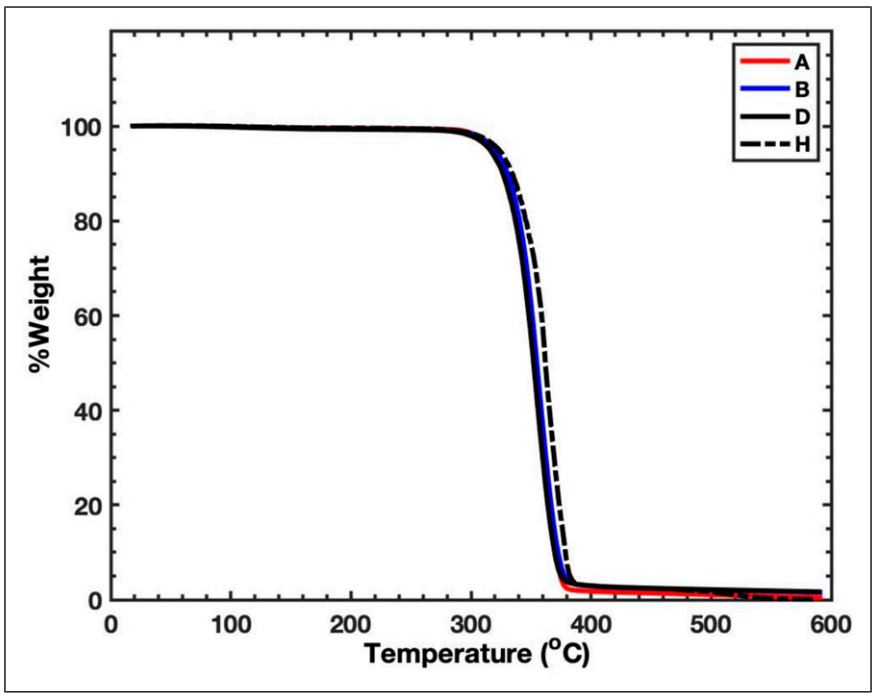

Figure 6. The thermogram of PLA/Chitosan/MCC composite.

temperatures obtained from the curves are not significantly different across all composites. The glass transition temperature is approximately 55–56°C, while the melting point is around 143–144°C. The composite H has wider, higher-melting-point peaks and therefore requires more thermal energy to melt. The values of the glass transition and melting temperatures are not very different from those of pure PLA reported in another work, with Tg = 50–64°C and Tm = 150–220°C.[75,76] Amorphous commercial PLA as a copolymer of PLLA is also reported to have Tg = 50–59.5°C and Tm = 129–171°C.[77]

The crystallinity of a polymer can also be obtained from DSC data using the following equation (1) below.[78]

$$X_c = \frac{\Delta H_m}{\Delta H_m^o} \times 100\% \tag{1}$$

In this equation, ΔH_m^o = the melting enthalpy of an ideal crystal, and ΔH_m = the melting enthalpy of the polymer. As shown in Table 3, although it appears amorphous in the XRD diffractogram (Figure 4), the composite is semi-crystalline, with a crystallinity of 23.70–29.47%. Higher crystallinity in the PLA/Chitosan/MCC composites is expected to imply enhanced the tensile strength of the FFF-fabricated specimens. The thermal properties obtained from DSC analysis confirm that all developed composites are suitable for FFF

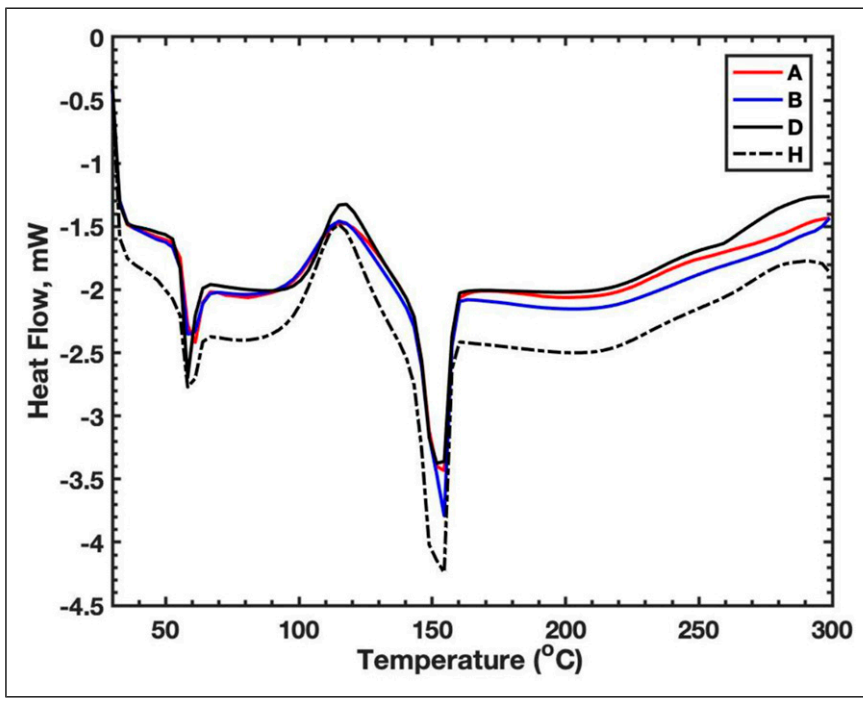

Figure 7. DSC curves of the studied PLA/Chitosan/MCC composites.

Table 3. Glass transition, melting temperature, melting enthalpy, and crystallinity of composites.

Composite	Tm (°C)	Tg (°C)	ΔH_m, J/g	X_C, %
A	144.1	56.10	22.05	23.70
B	143.4	55.48	23.93	25.73
D	143.8	55.24	23.90	25.70
H	143.0	55.63	27.41	29.47
Pure PLA[86]	130 – 180	50 – 80	93	100

filament applications, offering a good balance between processability and structural integrity.

Water Absorption Analysis

The preparation of water absorption test specimens began by cutting extruded filaments to a length of 25 ± 1 mm, with three specimens prepared for each composite composition. All test specimens were cleaned with ethanol, dried for at least 24 hours at 50°C, and then allowed to cool to room temperature. Each specimen was weighed using a balance with an accuracy of ±0.1 mg, and the measured value was recorded as the initial mass.

The water absorption of the specimens was measured by immersion in water at 23 ± 1°C. Each specimen was immersed in a container filled with distilled water, with a minimum volume of 300 mL per specimen (Figure 8).

The first weighing of the filament mass was conducted after 2 hours of immersion. Subsequent weighings were performed at 6, 24, and 48 hours of immersion. After each designated immersion period, the specimens were removed from the water, dried, weighed, and the measured value recorded. The weight of the specimen after 48 hours of immersion is recorded as the final mass. The water absorption data for each composite, obtained from the test results, are presented in Table 4.

Based on the test results, water absorption increased with increasing chitosan and MCC content. Composite D, which contains more chitosan than composite A, exhibited a higher water absorption capacity. This indicates that chitosan enhances the composite's water absorption. Similarly, composite B, which contains more MCC than composite A, absorbed more water. Although the increase in water absorption was not significantly different, this result indicates a positive influence of MCC on water absorption. An increase in extrusion temperature also enhanced the composites' water absorption. Composite H, which was processed at a higher extrusion temperature, exhibited higher water absorption compared to composite D. Overall, increasing the chitosan and MCC content, as well as increasing the extrusion temperature, resulted in increased water absorption of the composites.

The results are in line with previous research. A higher chitosan content tends to increase the composite's water absorption capacity, as chitosan is well known for its hydrophilic properties.[79] Adding MCC also reduces the composite's hydrophobicity.[80] Furthermore, changes in the polymer structure at higher processing temperatures may

Figure 8. Water absorption test.

Table 4. Water absorption test results.

Composite	Test	Water absorption (%)	Average (%)
A	First	0.5405	0.6012
	Second	0.5997	
	Third	0.6633	
B	First	0.5722	0.6096
	Second	0.8141	
	Third	0.4424	
D	First	0.9225	0.8422
	Second	0.9600	
	Third	0.6441	
H	First	0.3921	1.1163
	Second	1.0088	
	Third	1.9480	

reduce thermal stability or effective crosslinking, thereby making the material more susceptible to water penetration.[81] The diffusion of water molecules into the composite material alters its microstructure by forming internal voids within the polymer matrix.[82] Water diffusion into the composite also accelerates the degradation of PLA.[83] Water

absorption by PLA reduces the composite's mechanical strength by inducing PLA chain scission.[84]

When used as a filament material for FFF, the composite's water absorption must be carefully controlled. The composite should degrade within an appropriate time frame for its applications, but must not become brittle. Based on previous studies, the water absorption limit at saturation for PLA filaments is approximately 0.9% before severe hydrolytic degradation occurs during printing.[85] Therefore, composite H exhibits excessive moisture affinity, rendering it unsuitable for use as an FFF filament.

The performance of PLA/Chitosan/MCC composite filaments for FFF is governed by the interplay between composition, processing conditions, and interfacial interactions. Rheological analysis revealed that composites B and D exceeded the minimum melt flow index required for stable FFF printing. Composite A showed insufficient flowability, and composite H exhibited excessive water absorption, rendering both unsuitable for filament use. However, composite B exhibits critical structural defects due to insufficient interfacial compatibility between the high MCC loading and the PLA matrix. These findings highlight the importance of balancing filler content and processing temperature to achieve optimal extrusion performance. Overall, composite D (PLA 93 wt%, chitosan 2 wt%, MCC 5 wt%, extruded at 155°C) emerged as the most promising formulation, offering a favorable combination of melt flow behavior, thermal stability, interfacial cohesion, and controlled water absorption.

Conclusions

This research has developed PLA/Chitosan/MCC composite filaments for FFF applications via melt blending and extrusion. The results indicate that filament properties are significantly influenced by the balance between material composition and processing conditions. Chitosan acts as a compatibilizer that enhances interfacial adhesion through hydrogen bonding, while MCC contributes to structural reinforcement, despite its potential for agglomeration. Among all variations, the optimal composition was achieved with 93 wt% PLA, 2 wt% chitosan, and 5 wt% MCC at an extrusion temperature of 155°C, providing an ideal balance between processability, thermal stability, morphology, and water absorption. Future studies should focus on mechanical performance, antimicrobial efficacy, and in vitro degradation behavior to further validate the suitability of these composites for biomedical and orthopedic applications.

Author Contributions

T.J. Suteja: Funding acquisition, Conceptualization, Methodology, Investigation, Analysis, Writing Original Draft; N. Soeseno: Funding acquisition, Investigation, Analysis, Writing Original Draft; A. Fatmawati: Funding acquisition, Investigation, Analysis, Writing Original Draft; E. Savitri: Investigation, Analysis, Writing Original Draft; Y.P. Asmara: Analysis, Writing Original Draft.

Declaration of Conflicting Interests

The authors declare that they have no known financial or non-financial competing interests in any material discussed in this paper.

Funding

The authors disclosed receipt of the following financial support for the research, authorship, and/or publication of this article: This research was funded by the National Research and Innovation Agency (BRIN), Indonesia, through the RIIM Kompetisi grant under contract number 46/IV/KS/02/2025.

ORCID iD

The Jaya Suteja https://orcid.org/0000-0001-9090-8650

Data Availability Statement

The data that support the findings of this study are openly available in Repositori Ilmiah Nasional at https://hdl.handle.net/20.500.12690/RIN/3CPOKB. Data, including raw data, will be made available upon reasonable request to the corresponding author, in accordance with the National Research and Innovation Agency (BRIN) 's open data policies.

References

1. Nik MHNNK, Firdaus MKZH and Che HMK. Enhancing bone health in aging populations to prevent fragility fractures. *Int J Care Sch* 2023; 6: 1–6.
2. Rust A, Samade R, Campbell AB, et al. Time to surgery and outcomes following open reduction and internal fixation of both-bone forearm fractures. *Eur J Orthop Surg Traumatol* 2023; 34: 1–8. https://doi.org/10.1007/s00590-023-03560-8
3. Dhandapani R, Krishnan PD, Zennifer A, et al. Additive manufacturing of biodegradable porous orthopaedic screw. *Bioact Mater* 2020; 5: 458–467. https://doi.org/10.1016/j.bioactmat.2020.03.009
4. Solechan PRJ. Pengaruh penambahan material hidroksiapatit bovine dan polimer biodegradasi untuk meningkatkan kekuatan mekanik implan plate fiksasi internal tulang femur. *Pros Semin Nas NCIET Natl Conf Ind Eng Technol* 2020; 1: 108–117.
5. Al-Shalawi FD, Mohamed AAH, Jung DW, et al. Biomaterials as implants in the orthopedic field for regenerative medicine: metal versus synthetic polymers. *Polymers*; 15(12): 2601. https://doi.org/10.3390/polym15122601
6. Akay S and Yaghmur A. Recent advances in antibacterial coatings to combat orthopedic implant-associated infections. *Molecules*; 29(5): 1172. https://doi.org/10.3390/molecules29051172
7. Andrade MC, De Rus Aznar I, Brunnberg M, et al. Indications for the removal of implants after fracture healing: a comparison between human and veterinary medicine. *Vet Med* 2023; 68: 259–270. https://doi.org/10.17221/52/2023-vetmed

8. Montgomery BK, Gamble JG, Kha ST, et al. Indications for and risks associated with implant removal after pediatric trauma. *J Am Acad Orthop Surg Glob Res Rev* 2022; 6: 1–9. https://doi.org/10.5435/jaaosglobal-d-22-00050
9. Raheem AA, Hameed P, Whenish R, et al. A review on development of bio-inspired implants using 3d printing. *Biomimetics*; 6(4): 65. https://doi.org/10.3390/biomimetics6040065
10. Wang P, Gong Y, Zhou G, et al. Biodegradable implants for internal fixation of fractures and accelerated bone regeneration. *ACS Omega* 2023; 8: 27920–27931. https://doi.org/10.1021/acsomega.3c02727
11. Agarwal R, Gupta V and Singh J. Additive manufacturing-based design approaches and challenges for orthopaedic bone screws: a state-of-the-art review. *J Brazilian Soc Mech Sci Eng* 2022; 44: 1–25. https://doi.org/10.1007/s40430-021-03331-8
12. Aihemaiti P, Jiang H, Aiyiti W, et al. Optimization of 3D printing parameters of biodegradable polylactic acid/hydroxyapatite composite bone plates. *Int J Bioprinting* 2022; 8: 153–166. https://doi.org/10.18063/ijb.v8i1.490
13. Ebrahimi F and Ramezani Dana H. Poly lactic acid (PLA) polymers: from properties to biomedical applications. *Int J Polym Mater Polym Biomater* 2022; 71: 1117–1130. https://doi.org/10.1080/00914037.2021.1944140
14. Huang B, Yang M, Kou Y, et al. Absorbable implants in sport medicine and arthroscopic surgery: a narrative review of recent development. *Bioact Mater* 2024; 31: 272–283. https://doi.org/10.1016/j.bioactmat.2023.08.015
15. Pisecky L, Luger M, Klasan A, et al. Bioabsorbable implants in forefoot surgery: a review of materials, possibilities and disadvantages. *EFORT Open Rev* 2021; 6: 1132–1139. https://doi.org/10.1302/2058-5241.6.200157
16. Sandanamsamy L, Mogan J, Halim NA, et al. A review on 3D printing bio-based polymer composite. *IOP Conf Ser Mater Sci Eng* 2021; 1078: 012031. https://doi.org/10.1088/1757-899x/1078/1/012031
17. Wu Y, Gao X, Wu J, et al. Biodegradable polylactic acid and its composites: characteristics, processing, and sustainable applications in sports. *Polymers* 2023; 15(14): 3096. https://doi.org/10.3390/polym15143096
18. Kovylin RS, Aleynik DY and Fedushkin IL. Modern porous polymer implants: synthesis, properties, and application. *Polym Sci - Ser C* 2021; 63: 29–46. https://doi.org/10.1134/s1811238221010033
19. Tappa K, Jammalamadaka U, Weisman JA, et al. 3D printing custom bioactive and absorbable surgical screws, pins, and bone plates for localized drug delivery. *J Funct Biomater*; 10. https://doi.org/10.3390/jfb10020017
20. DeStefano V, Khan S and Tabada A. Applications of PLA in modern medicine. *Eng Regen* 2020; 1: 76–87. https://doi.org/10.1016/j.engreg.2020.08.002
21. Hui I, Pasquier E, Solberg A, et al. Biocomposites containing poly(lactic acid) and chitosan for 3D printing – assessment of mechanical, antibacterial and in vitro biodegradability properties. *J Mech Behav Biomed Mater* 2023; 147: 106136. https://doi.org/10.1016/j.jmbbm.2023.106136
22. Suryanegara L, Fatriasari W, Zulfiana D, et al. Novel antimicrobial bioplastic based on PLA-Chitosan by addition of TiO2 and ZnO. *J Environ Health Sci Eng* 2021; 19: 415–425. https://doi.org/10.1007/s40201-021-00614-z

23. Ke CL, Deng FS, Chuang CY, et al. Antimicrobial actions and applications of chitosan. *Polymers*; 13(6): 904. https://doi.org/10.3390/polym13060904
24. Shiva S, Asuwin Prabu RG, Bajaj G, et al. A review on the recent applications of synthetic biopolymers in 3D printing for biomedical applications. *J Mater Sci Mater Med*; 34. https://doi.org/10.1007/s10856-023-06765-9
25. Yan D, Li Y, Liu Y, et al. Antimicrobial properties of chitosan and chitosan derivatives in the treatment of enteric infections. *Molecules*; 26(23): 7136. https://doi.org/10.3390/molecules26237136
26. Singh S, Singh G, Prakash C, et al. 3D printed biodegradable composites: an insight into mechanical properties of PLA/Chitosan scaffold. *Polym Test* 2020; 89: 106722. https://doi.org/10.1016/j.polymertesting.2020.106722
27. Ranjan N, Singh R, Ahuja IPS, et al. In: AlMangour B (ed). *Fabrication of PLA-HAp-CS Based Biocompatible and Biodegradable Feedstock Filament Using Twin Screw Extrusion*. Cham: Springer International Publishing, pp. 325–345.
28. Singh R, Singh G, Singh J, et al. Investigations for tensile, compressive and morphological properties of 3D printed functional prototypes of PLA-PEKK-HAp-CS. *J Thermoplast Compos Mater* 2021; 34: 1408–1427. https://doi.org/10.1177/0892705719870595
29. Abifarin JK, Prakash C and Singh S. Optimization and significance of fabrication parameters on the mechanical properties of 3D printed Chitosan/PLA scaffold. *Mater Today Proc* 2021; 50: 2018–2025. https://doi.org/10.1016/j.matpr.2021.09.386
30. Goetjes V, von Boyneburgk CL, Heim HP, et al. Influence of chitosan and grape seed extract on thermal and mechanical properties of PLA blends. *Polymers*; 15(6): 1570. https://doi.org/10.3390/polym15061570
31. Li Y, Huang L, Wang X, et al. Blending and functionalisation modification of 3D printed polylactic acid for fused deposition modeling. *Rev Adv Mater Sci*; 62. https://doi.org/10.1515/rams-2023-0140
32. Suteja TJ, Firmanto H, Soesanti A, et al. Properties investigation of 3D printed continuous pineapple leaf fiber-reinforced PLA composite. *J Thermoplast Compos Mater* 2022; 35: 2052–2061. https://doi.org/10.1177/0892705720945371
33. dos Santos FA, Iulianelli GCV and Tavares MIB. Effect of microcrystalline and nanocrystals cellulose fillers in materials based on PLA matrix. *Polym Test* 2017; 61: 280–288. https://doi.org/10.1016/j.polymertesting.2017.05.028
34. Aziz T, Haq F, Farid A, et al. Challenges associated with cellulose composite material: Facet engineering and prospective. *Environ Res* 2023; 223: 115429. https://doi.org/10.1016/j.envres.2023.115429
35. Ganapathy V, Muthukumaran G, Sudhagar PE, et al. Mechanical properties of cellulose-based multiscale composites: a review. *Polym Compos* 2023; 44: 734–756. https://doi.org/10.1002/pc.27175
36. Xian X, Wang X, Zhu Y, et al. Effects of MCC content on the structure and performance of PLA/MCC biocomposites. *J Polym Environ* 2018; 26: 3484–3492. https://doi.org/10.1007/s10924-018-1226-3
37. Arockiam AJ, Subramanian K, Padmanabhan RG, et al. A review on PLA with different fillers used as a filament in 3D printing. *Mater Today Proc* 2021; 50: 2057–2064.

38. Mohan BS, Kumar A and Katiyar V. Microcrystalline cellulose, polylactic acid and polypropylene biocomposites and its morphological, mechanical, thermal and rheological properties. *Composites, Part B Eng* 2020; 184: 107717.
39. Selwin M, Nagarajan R, Ponsuriyaprakash S, et al. Optimization of wear behavior of additively manufactured green biocomposites from printed polylactic acid (PLA) and microcrystalline cellulose. *Wood Mater Sci Eng* 2025; 21: 1–10. https://doi.org/10.1080/17480272.2025.2466226
40. Omran AAB, Mohammed AABA, Sapuan SM, et al. Micro-and nanocellulose in polymer composite materials: a review. *Polymers* 2021; 13: 1–30. https://doi.org/10.3390/polym13020231
41. Ahmad ND, Kusmono WMW, et al. Preparation and properties of cellulose nanocrystals-reinforced poly (lactic acid) composite filaments for 3D printing applications. *Results Eng* 2023; 17: 100842. https://doi.org/10.1016/j.rineng.2022.100842
42. Strnad S and Zemljič LF. Cellulose–chitosan functional biocomposites. *Polymers* 2023; 15: 425. https://doi.org/10.3390/polym15020425
43. Hasnida Raja Hashim R, Anas Nagoor Gunny A, Sung TS, et al. The effect nanofillers on the functional properties of pla and chitosan based film (kesan pengisian nano kepada sifat filem yang berasaskan asid polilatik dan kitosan). *Malays J Anal Sci* 2023; 27: 63–73.
44. Lacambra-Andreu X, Maazouz A, Lamnawar K, et al. A review on manufacturing processes of biocomposites based on Poly(α-Esters) and bioactive glass fillers for bone regeneration. *Biomimetics*; 8: 8010081. https://doi.org/10.3390/biomimetics8010081
45. Husain M, Singh R and Pabla BS. A review on 3D printing of partially absorbable implants. *J Inst Eng Ser C* 2023; 104: 1113–1132. https://doi.org/10.1007/s40032-023-00980-7
46. Moosabeiki V, de Winter N, Cruz SM, et al. 3D printed patient-specific fixation plates for the treatment of slipped capital femoral epiphysis: topology optimization vs. conventional design. *J Mech Behav Biomed Mater* 2023; 148: 106173. https://doi.org/10.1016/j.jmbbm.2023.106173
47. Skelley NW. Design and development of a novel 3-D printed external fixation device for fracture stabilization. *3D Print Med* 2023; 9: 1–13. https://doi.org/10.1186/s41205-023-00179-7
48. Wixted CM, Peterson JR, Kadakia RJ, et al. Three-dimensional printing in orthopaedic surgery: current applications and future developments. *J Am Acad Orthop Surg Glob Res Rev* 2021; 5: E200023011. https://doi.org/10.5435/jaaosglobal-d-20-00230
49. Ballard DH, Tappa K, Boyer CJ, et al. Antibiotics in 3D-printed implants, instruments and materials: benefits, challenges and future directions. *J 3D Print Med* 2019; 3: 83–93. https://doi.org/10.2217/3dp-2019-0007
50. Zglobicka I, Joka-Yildiz M, Molak R, et al. Poly(lactic acid) matrix reinforced with diatomaceous Earth. *Materials* 2022; 15: 1–11. https://doi.org/10.3390/ma15186210
51. Onumah J, Afoakwah NA, Boamah PO, et al. Biological properties and application of chitosan and low molecular weight chitosan in food industry: a review. *Carbohydr Res* 2025; 552: 109475. https://doi.org/10.1016/j.carres.2025.109475
52. Ramires EC, Megiatto JD, Dufresne A, et al. Cellulose nanocrystals versus microcrystalline cellulose as reinforcement of lignopolyurethane matrix. *Fibers*; 8: 21. https://doi.org/10.3390/fib8040021

53. Rahaman H, Habib R, Hosen S, et al. Different amounts of chitosan on the morphological, thermal and antibacterial properties of poly (L -lactic acid)/microcrystalline cellulose biopolymer composites. *Mater Int* 2020; 2: 402–411.
54. Krapež Tomec D, Schwarzkopf M, Repič R, et al. Effect of thermal modification of wood particles for wood-PLA composites on properties of filaments, 3D-printed parts and injection moulded parts. *Eur J Wood Wood Prod* 2024; 82: 403–416. https://doi.org/10.1007/s00107-023-02018-2
55. Srihanam P, Phromsopha T, Sangdee A, et al. Thermo-compression of thermoplastic chitosan films reinforced with microcrystalline cellulose for antibacterial food packaging application. *Polymers* 2025; 17: 1–20. https://doi.org/10.3390/polym17182460
56. Patti A and Acierno S. Rheological changes in bio-based filaments induced by extrusion-based 3D printing process. *Materials*; 17: 3839. https://doi.org/10.3390/ma17153839
57. Wang S, Capoen L, D'hooge DR, et al. Can the melt flow index be used to predict the success of fused deposition modelling of commercial poly(lactic acid) filaments into 3D printed materials? *Plast Rubber Compos* 2018; 47: 9–16. https://doi.org/10.1080/14658011.2017.1397308
58. Farah S, Anderson DG and Langer R. Physical and mechanical properties of PLA, and their functions in widespread applications — a comprehensive review. *Adv Drug Deliv Rev* 2016; 107: 367–392. https://doi.org/10.1016/j.addr.2016.06.012
59. Gorgun E, Ali A and Islam MS. Biocomposites of Poly(Lactic acid) and microcrystalline cellulose: influence of the coupling agent on thermomechanical and absorption characteristics. *ACS Omega* 2024; 9: 11523–11533. https://doi.org/10.1021/acsomega.3c08448
60. He Z, Nam S, Kulkarni S, et al. Thermal evaluation of biocomposites made from Poly(Lactic acid) and cottonseed byproducts. *Macromolecules* 2025; 5: 1–17. https://doi.org/10.3390/macromol5020016
61. Flores-León JR, Rodríguez-Félix DE, Quiroz-Castillo JM, et al. Effect of degradation on the physicochemical and mechanical properties of extruded films of poly(lactic acid) and chitosan. *ACS Omega* 2024; 9: 9526–9535. https://doi.org/10.1021/acsomega.3c09296
62. Vasu VK. Structurally tuned PLA chitosan composites through cryogenic mechanochemistry for biofunctional material development. *J Eng Appl Sci* 2025; 72: 1–21. https://doi.org/10.1186/s44147-025-00812-8
63. Sandanamsamy L, Harun WSW, Ishak I, et al. A comprehensive review on fused deposition modelling of polylactic acid. *Progr Addit Manuf* 2023; 8: 775–799. https://doi.org/10.1007/s40964-022-00356-w
64. Shang Y, Xu Q, Jiang B, et al. Slowing crystallization to enhance interlayer strength of 3D printed poly (ether ether ketone) parts by molecular design. *Addit Manuf* 2022; 59: 103104. https://doi.org/10.1016/j.addma.2022.103104
65. Mazzanti V, Pariante R, Bonanno A, et al. Reinforcing mechanisms of natural fibers in green composites: role of fibers morphology in a PLA/Hemp model system. *Compos Sci Technol* 2019; 180: 51–59. https://doi.org/10.1016/j.compscitech.2019.05.015
66. Fatmawati A, Nurtono T and Widjaja A. Thermogravimetric kinetic-based computation of raw and pretreated coconut husk powder lignocellulosic composition. *Bioresour Technol Rep* 2023; 22: 101500. https://doi.org/10.1016/j.biteb.2023.101500

67. Fortunati E, Peltzer M, Armentano I, et al. Combined effects of cellulose nanocrystals and silver nanoparticles on the barrier and migration properties of PLA nano-biocomposites. *J Food Eng* 2013; 118: 117–124. https://doi.org/10.1016/j.jfoodeng.2013.03.025
68. Oksman K, Mathew AP, Siqueira G, et al. *Accepted manuscript*.
69. Rhim J-W, Park H-M and Ha C-S. Bio-nanocomposites for food packaging applications. *Prog Polym Sci* 2013; 38: 1629–1652. https://doi.org/10.1016/j.progpolymsci.2013.05.008
70. Pan R, Yu E, Wang Y, et al. Phytic acid and melamine-modified microcrystalline cellulose as effective flame retardants in polylactic acid composites. *Carbohydr Polym* 2025; 368: 124087. https://doi.org/10.1016/j.carbpol.2025.124087
71. Wu B, Abdalkarim SYH, Li Z, et al. Synergistic enhancement of high-barrier polylactic acid packaging materials by various morphological carbonized cellulose nanocrystals. *Carbohydr Polym* 2025; 351: 123118. https://doi.org/10.1016/j.carbpol.2024.123118
72. Seno Flores JD, de AAT, Lopes Vieira Cunha DA, et al. Sustainable polymer reclamation: recycling poly(ethylene terephthalate) glycol (PETG) for 3D printing applications. *J Mater Sci Mater Eng*; 19. https://doi.org/10.1186/s40712-024-00163-x
73. Jacob J, Linson N, Mavelil-Sam R, et al. *Poly(lactic acid)/nanocellulose biocomposites for sustainable food packaging*. Netherlands: Springer, 2024. https://doi.org/10.1007/s10570-024-05975-w
74. Wohlert M, Benselfelt T, Wågberg L, et al. Cellulose and the role of hydrogen bonds: not in charge of everything. *Cellulose* 2022; 29: 1–23. https://doi.org/10.1007/s10570-021-04325-4
75. Moldovan A, Sarosi I, Cuc S, et al. Development and characterization of PLA food packaging composite. *J Therm Anal Calorim* 2025; 150: 2469–2481. https://doi.org/10.1007/s10973-024-13841-x
76. Ranjan N, Singh R, Ahuja IPS, et al. 3D printed scaffolds for tissue engineering applications: mechanical, morphological, thermal, in-vitro and in-vivo investigations. *CIRP J Manuf Sci Technol* 2021; 32: 205–216. https://doi.org/10.1016/j.cirpj.2021.01.002
77. Molinari G, Parlanti P, Passaglia E, et al. Dependence of the crystal structure on the D-units amount in semi-crystalline poly(lactic acid). *Int J Biol Macromol* 2024; 281: 136296. https://doi.org/10.1016/j.ijbiomac.2024.136296
78. Doumeng M, Makhlouf L, Berthet F, et al. A comparative study of the crystallinity of polyetheretherketone by using density, DSC, XRD, and raman spectroscopy techniques. *Polym Test*; 93: 106878. https://doi.org/10.1016/j.polymertesting.2020.106878
79. Jayanudin LRSD, Barleany DR, et al. Chitosan-graft-poly(acrylic acid) superabsorbent's water holding in sandy soils and its application in agriculture. *Polymers* 2022; 14: 1–14.
80. Samat N, Lazim NHM and Halim Z. Dynamic mechanical and water absorption properties of microcrystalline cellulose reinforced polypropylene composites: the effect of unconventional irradiation route. *IIUM Eng J* 2019; 20: 188–196.
81. Sabet-Bokati K and Plucknett K. Water-induced failure in polymer coatings: mechanisms, impacts and mitigation strategies—A comprehensive review. *Polym Degrad Stabil* 2024; 230: 111058. https://doi.org/10.1016/j.polymdegradstab.2024.111058
82. da Silva D, Kaduri M, Poley M, et al. Biocompatibility, biodegradation and excretion of polylactic acid (PLA) in medical implants and Theranostic systems. *Chem Eng J (Amsterdam, Neth)* 2018; 340: 9–14. https://doi.org/10.1016/j.cej.2018.01.010

83. Limsukon W, Rubino M, Rabnawaz M, et al. Hydrolytic degradation of poly(lactic acid): unraveling correlations between temperature and the three phase structures. *Polym Degrad Stabil* 2023; 217: 110537. https://doi.org/10.1016/j.polymdegradstab.2023.110537
84. Ainin FN, Azaman MD, Abdul Majid MS, et al. The influence of water absorption on the mechanical performance of 3D-printed sandwich composite structures made from PLA-based materials under quasi-static loading conditions. *Polym Compos* 2025; 46: 6221–6240. https://doi.org/10.1002/pc.29355
85. Banjo AD, Agrawal V, Auad ML, et al. Moisture-induced changes in the mechanical behavior of 3D printed polymers. *Composer Part C Open Access* 2022; 7: 100243. https://doi.org/10.1016/j.jcomc.2022.100243
86. Castro-Aguirre E, Iñiguez-Franco F, Samsudin H, et al. Poly(lactic acid)—Mass production, processing, industrial applications, and end of life. *Adv Drug Deliv Rev* 2016; 107: 333–366. https://doi.org/10.1016/j.addr.2016.03.010